The effect of intermittent lubrication on the fatigue life of pearlitic rail steel in rolling–sliding contact

D I Fletcher* and **J H Beynon**
Department of Mechanical Engineering, The University of Sheffield, UK

Abstract: Railway flange lubrication can be unreliable, resulting in intermittent rather than continuous lubrication. Twin-disc contact simulation tests were carried out to investigate the influence of intermittent lubrication on rail steel fatigue life, using both a colloidal suspension of molybdenum disulphide in an oil carrier fluid (similar to a commercial flange lubrication product) and water. A brief interruption of the lubricant supply during molybdenum disulphide lubrication produced rapid surface failure of the rail steel, which was followed by rapid contact fatigue crack growth upon reapplication of the lubricant. During water lubrication the interruption of the lubricant (water) supply did not produce such rapid crack growth. The results were found to be in qualitative agreement with the predictions of the three-mechanism model of rolling contact fatigue, which combines the mechanisms of ratchetting (accumulation of unidirectional plastic strain until the critical failure strain of the material is reached) and the fracture mechanics-based mechanisms of shear stress driven and tensile fluid assisted crack growth. Analysis of the test results using this model revealed crack face friction to be an important factor controlling crack growth, which may be responsible for the difference in behaviour between contacts lubricated with the molybdenum disulphide-based lubricant and those lubricated by water.

Keywords: rolling contact fatigue, flange lubrication, pearlitic rail steel

NOTATION

E	Young's modulus
k	shear yield strength
$K_{\sigma,\tau}$	equivalent tensile and shear stress intensity factors
$K_{\sigma\text{th},\tau\text{th}}$	threshold stress intensity factors for tensile and shear mode crack growth
$N_{\text{R,W}}$	disc specimen revolutions for rail and wheel discs respectively
p_0	maximum Hertzian contact pressure
p_r	ratchetting stress, varying with depth z, defined by equation (3)
p_s	general shakedown parameter, varying with depth z, defined by equation (4)
p_s^A	shakedown parameter p_s for a specific contact condition [A =D (dry), M (MIO lubrication), W (water lubrication)]
P	contact load per unit contact length
r_cyclic	cyclic plastic zone radius, defined by equation (5)
R	reduced radius of contact, defined as $1/R = 1/R_\text{R} + 1/R_\text{W}$
$R_\text{R,W}$	rail and wheel radii
μ_cf	crack face friction coefficient
μ_surface	contact surface friction coefficient, equal to the traction coefficient for a fully sliding contact
σ_y	tensile yield strength
$\tau_{zx,\text{max}}$	maximum absolute value of the orthogonal shear stress experienced by the rail steel during the passage of a wheel disc contact

The MS was received on 22 October 1999 and was accepted after revision for publication on 31 January 2000.
** Corresponding author: Department of Mechanical Engineering, The University of Sheffield, Mappin Street, Sheffield S1 3JD, UK.*

1 INTRODUCTION

Lubrication of the rail–wheel contact may take place owing to rain (water lubrication) or by application of flange lubrication products to reduce wear of the rail and wheel, which may otherwise be severe in curves owing to the high degree of sliding that takes place when the wheel flange and rail gauge face make contact [**1**]. Rain inherently produces intermittent lubrication of the rail–wheel contact, but it is found that flange lubrication may also be interrupted for a variety of reasons such as infrequent maintenance of remote track-based lubricators and removal of lubricants from the track by rain

[2, 3]. Previous investigations have shown that both water and liquid-based flange lubrication products may contribute to rail rolling contact fatigue (RCF) failures by mechanisms such as crack face friction modification and fluid entrapment [4–6]. It was therefore decided to investigate the influence of discontinuous lubrication on the RCF life of pearlitic rail steel.

Laboratory-based twin-disc tests were conducted using both water lubrication and molybdenum disulphide dispersed in an oil carrier (MIO) which is similar to a commercial flange lubrication product. It was found that an unusually rapid failure of the rail disc surface occurred during unlubricated cycles following MIO lubrication, but that during water lubrication the rail fatigue life was virtually independent of the distribution of unlubricated cycles among water lubricated cycles. To examine the test results, the three mechanism (TM) model of rolling contact fatigue [7] was applied, which combines the mechanisms of crack growth by ratchetting (accumulation of unidirectional plastic strain until the critical failure strain of the material is reached) with shear and tensile mechanisms of crack growth described by fracture mechanics.

Very few investigations into the intermittent application of lubricants could be found. Tyfour *et al.* [8] used a twin disc contact simulation to investigate the effect on rail RCF life of a period of dry contact preceding a period of water lubrication. For a contact operating with a maximum Hertzian contact pressure of 1500 MPa it was found that 200 initial dry cycles gave a reduction in fatigue life to 87 per cent of the value found in a test with water lubrication throughout, while 500 dry cycles reduced the fatigue life to 40 per cent of its previous value. The reduction in fatigue life brought about by high-traction unlubricated cycles was attributed to the increased rate of ratchetting strain accumulation at the surface of the rail disc, compared with that during lower-traction water lubricated cycles.

A rail–wheel contact undergoing repeated application and removal of water lubrication was studied by Kaneta *et al.* [9]. Contacts were run dry or wet throughout testing, dry then wet, wet then dry, and in a repeating pattern of dry and wet periods, and it was found that a RCF squat defect may be produced only by repeated application of dry and wet cycles. Theoretical explanation of the findings of this experimental work rely on the fracture mechanics approach to rolling contact fatigue developed by Murakami *et al.* [10] and Kaneta *et al.* [11], on which the fracture mechanics-based shear and tensile mechanisms of the TM model are based.

2 PROCEDURE

2.1 Experimental equipment

It was decided to use the SUROS (Sheffield University ROlling Sliding) twin-disc contact testing machine, which is described by Fletcher and Beynon [12]. This machine uses the line contact between two independently driven cylindrical test specimens to simulate the normal load and longitudinal slip present at a rail–wheel contact. However, the lateral and spin creep that may be present at the rail–wheel contact cannot be simulated. The twin-disc simulation method is useful for the investigation of RCF failures because these are typically found in straight track or in shallow curves where rail–wheel contact is dominated by a combination of normal load and longitudinal slip, but where lateral and spin creepages are relatively low. The twin-disc testing configuration has previously been used in the investigation of rail RCF by, for example, Beynon *et al.* [13] and Clayton and Su [14].

The SUROS machine is based on a Colchester Mascot 1600 lathe, with the specimens held using machine tool arbours mounted in bearings held by castings secured to the machine bed mid-way along its length. The rail specimen is driven by the lathe motor and gearbox, while the wheel specimen is driven by a separate 7 kW a.c. motor mounted at the tailstock end of the machine bed. Normal load is applied to the discs by a hydraulic piston and is measured by a load cell mounted in line with the piston. Torque due to rolling–sliding contact between the specimens is measured by a transducer secured to the drive shaft of the rail specimen, enabling the traction coefficient (the ratio of tractive to normal forces transmitted by the contact) to be measured. Disc speeds and numbers of revolutions are measured by shaft encoders fitted in line with the drive shafts. Specimens for use on the machine are manufactured to the drawing shown in Fig. 1a, and are removed from the parent rail and wheel components as shown in Fig. 1b. The machine is shown schematically in Fig. 1c.

During testing, crack detection is by a non-contact eddy current method using the Elotest® B1 commercial crack detection unit with a probe which is scanned across the surface of the specimen to detect cracks at any location [15]. The unit is calibrated using a disc containing a spark eroded crack, and a signal trigger level is then set to define the fatigue life for the tests. Prior to each test, both the rail and wheel discs are cleaned in an ultrasonic bath of ethanol, and they are then examined using the eddy current probe to ensure that no significant defects are present.

2.2 Contact conditions and test sequences

The maximum Hertzian contact pressure in the line contact between the test discs is calculated using the equation developed by Timoshenko and Goodier [16]

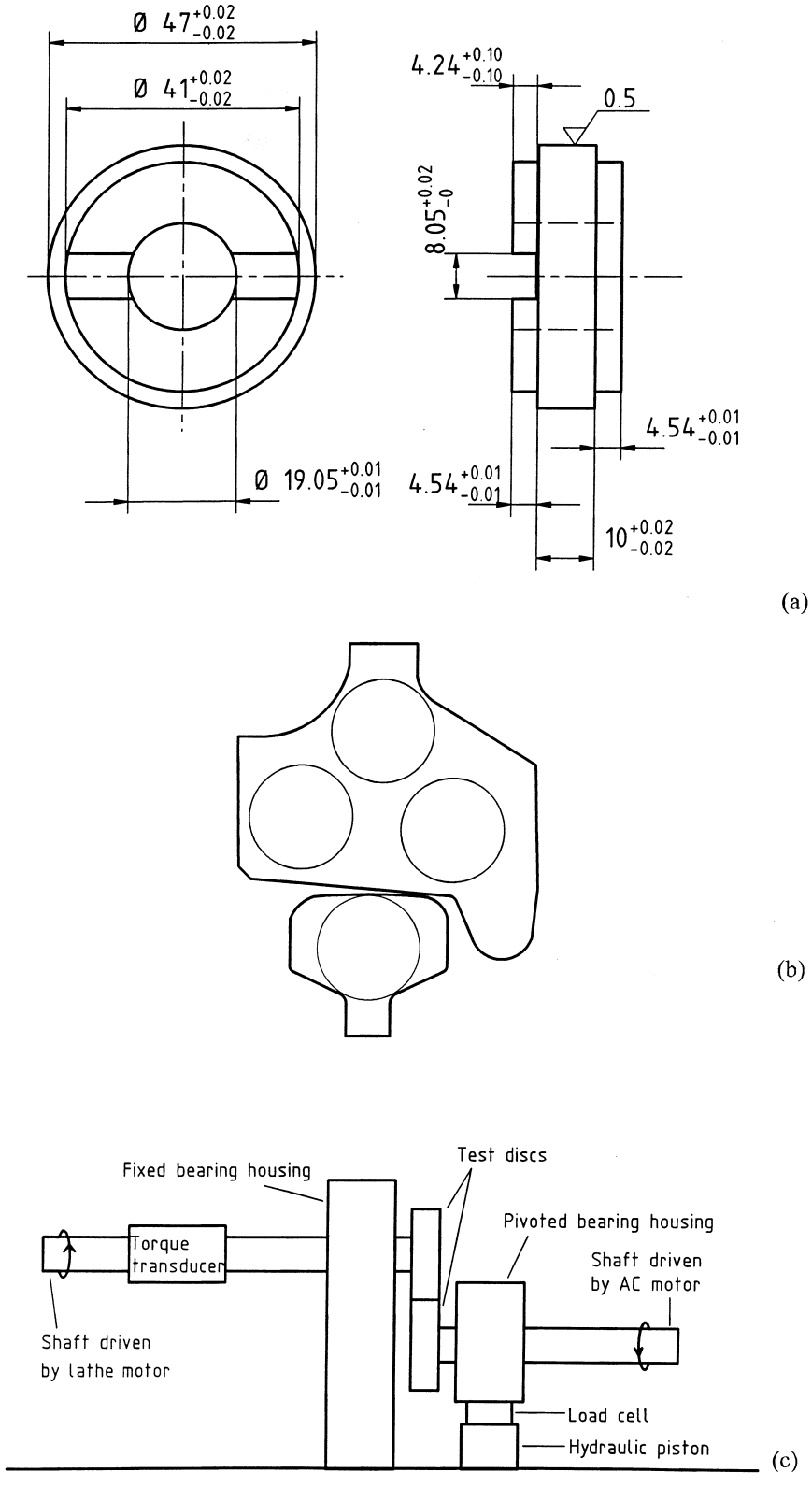

Fig. 1 (a) SUROS test specimen dimensions (in mm), (b) typical locations of test specimens in cross-sections of the wheel and rail and (c) schematic representation of the SUROS machine

for two elastically identical steel cylinders. Maximum Hertzian contact pressure is given by

$$p_0 = 0.418\sqrt{\frac{PE}{R}} \tag{1}$$

The slip ratio (in per cent), representing the ratio of sliding to rolling distances over the entire test, is defined as

$$\text{Slip} = 200\left(\frac{R_W N_W - R_R N_R}{R_R N_R + R_W N_W}\right) \tag{2}$$

All tests took place with 1 per cent slip at a nominal speed of 400 r/min and with a maximum Hertzian contact pressure of 1500 MPa. This contact pressure is representative of that found at the contact between a locomotive driving wheel and the railhead. At this location, Kalousek [**17**] showed contact pressure could vary within the range 830–3000 MPa, depending on the rail and wheel profile and the contact patch location, although Barwell [**18**] estimated it to be typically 1200 MPa. The value of slip was based on work by Bolton and Clayton [**19**] which showed that for a valid simulation the slip at the contact need only be increased to the level at which the limiting friction force is achieved. For a rail–wheel contact, Greenwood [**20**] has shown that this occurs at approximately 1 per cent slip, and this is also the case for the twin-disc SUROS simulation. Although flange lubrication of the rail usually takes place on the rail gauge face, it was decided that railhead contact conditions would represent the worst case of lubricant migration on to the railhead, which is where potentially dangerous RCF failures are most often initiated. It is also the region in which rain water may be expected to influence RCF crack growth.

Following consideration of the work reported by Tyfour *et al*. [**8**], it was decided to use 500 unlubricated cycles during each test, and to examine how rail disc fatigue life would be affected by the distribution of these 500 dry cycles among the lubricated cycles. The distributions used are shown in Table 1 and were devised to take into account that the fatigue life during water lubrication is generally lower than during MIO lubrication. Additional tests were included to examine crack growth following particular lubrication sequences without continuing to run until the defined fatigue life of the disc. Table 1 also shows the rail and wheel steel material codes for each test. Although the steels used unavoidably differed between the tests, the chemical composition and mechanical properties (Table 2) were very similar in each case.

Tests W1 to W4 took place under identical conditions to allow estimation of the repeatability of fatigue life determination when using the SUROS machine, and they are discussed in that context elsewhere [**12**]. Only average results for these tests are presented here.

Table 2 Chemical composition and mechanical properties of the rail and wheel steels

	Code			
Composition (wt %)	BS11 rail	NG96 rail	W8A wheel	WH268 wheel
Carbon	0.52	0.55	0.64	0.55
Silicon	0.2	0.26	0.23	0.27
Manganese	1.07	1.05	0.71	0.75
Nickel	0.03	0.03	0.17	0.20
Chromium	<0.01	0.03	0.18	0.26
Molybdenum	<0.01	0.003	0.03	0.08
Sulphur	0.018	0.022	0.041	0.018
Phosphorus	0.013	0.011	0.023	0.011
Vickers hardness (HV 500 g)	245	235	275	270
Ultimate tensile strength (MPa)	781	820	857	906
Tensile yield strength (MPa)	406	430	325	573*

* 0.2% proof stress.

Table 1 Test codes, sequences of lubricant application and the steels used in each test

Test code	Rail steel/wheel steel	Test sequence
M1	NG96/WH268	25 000MIO
M2	BS11/WH268	500D, Lubrication using MIO until failure
M3	BS11/WH268	250D, 25 000MIO, 250D, Lubrication using MIO until failure
M4	NG-96/WH268	250D, 25 000MIO, 250D, Lubrication using MIO until failure
M5	NG-96/WH268	250D, 25 000MIO, 250D, Lubrication using MIO until failure
M6	NG-96/WH268	25 000MIO, 250D
W1–W4	BS11/W8A	500D, Lubrication using water until failure
W5	BS11/WH268	250D, 6000W, 250D, Water until failure
W6	BS11/WH268	125D, 2000W, 125D, 2000W, 125D, 2000W, 125D, Water until failure
W7	NG-96/WH268	6000W
W8	NG-96/WH268	6000W, 250D
D1	BS11/WH268	250D
D2	BS11/WH268	500D

Numbers are rail disc cycles; W = water lubricated cycles; MIO = molybdenum disulphide suspended in oil lubricated cycles; D = unlubricated dry cycles. All tests took place at 1500 MPa maximum Hertzian contact pressure.

2.3 Intermittent lubrication

Removal of lubricant from the test disc surfaces was required during tests in which a period of dry contact followed either water or MIO lubrication. For water lubricated discs it was found that, if the machine was stopped, the water could quickly be removed from the test discs by a warm air blower, and the test could then continue. For the oil-based lubricant MIO it was necessary to use a specialist solvent (Ronseal Tri-flow Orange 2) to remove the lubricant, and then to use ethanol to remove all traces of the solvent. This was carried out using a series of clean cloths, while the test samples remained on the SUROS machine, and was successful in cleaning the surface of the discs. However, for test M5 it was decided to use an ultrasonic cleaning method in which the discs were immersed in a beaker of solvent for 30 min and then in a beaker of ethanol for a similar period, both beakers being placed in an ultrasonic bath.

2.4 Three mechanism model of rolling contact fatigue

The three mechanisms of crack growth considered by the TM model are ratchetting (mechanism R) and shear and tensile modes of crack growth described by fracture mechanics (mechanisms S and T respectively). Mechanism R is dependent on the plastic deformation of the rail surface that takes place during initial wheel passes which load the rail steel beyond its yield strength [**21**]. However, the increment in plastic strain with each successive contact pass is reduced as the material undergoes 'shakedown'. A completely elastic state may be reached at applied loads below the elastic shakedown limit of the rail, but loads above the plastic shakedown limit (ratchetting threshold) will lead to continued incremental increases in rail steel plastic deformation (ratchetting) with each contact pass. Although the ratchetting process describes accumulation of plastic deformation, the ductility of the rail steel is finite. Steel that reaches the limit of its ductility undergoes ductile fracture and breaks away from the main body of the rail [**22**], producing a crack without the requirement for a pre-existing flaw to be present in the material. The stress driving the ratchetting process, p_r [equation (3)], depends on the difference between the maximum Hertzian contact pressure, p_0, and the shakedown parameter, p_s [equation (4)], which can be calculated using the relationship previously applied to unlubricated contacts by Fletcher and Beynon [**23**]:

$$p_r = p_0 - p_s \tag{3}$$

$$p_s = \frac{p_0 k}{(\tau_{zx,\max})_z} \tag{4}$$

Figure 2 shows the variation in p_s with depth beneath the contact surface, indicating the maximum contact pressure that may be applied to the contact surface without producing additional plastic deformation of the

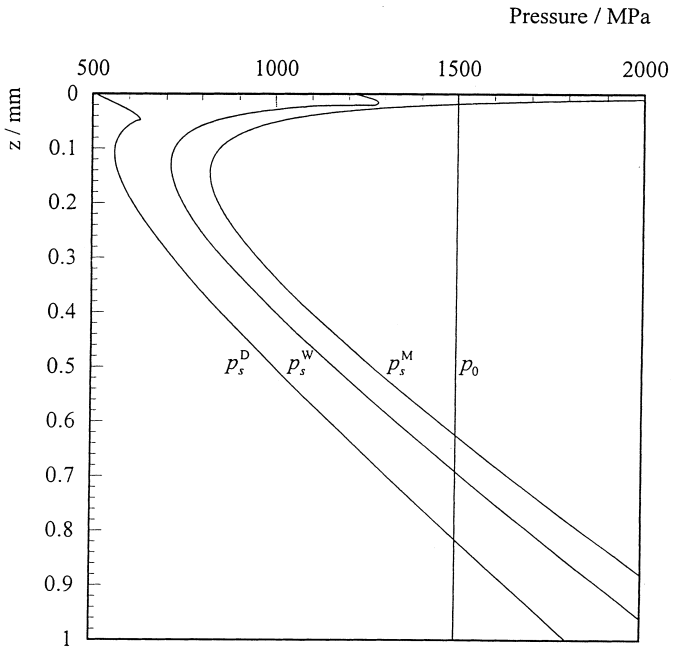

Fig. 2 Shakedown parameter p_s and maximum Hertzian contact pressure p_0 for unlubricated (p_s^D), water lubricated (p_s^W) and MIO lubricated (p_s^M) tests. Strain accumulation (ratchetting) at any depth is dependent on the difference between the applied contact pressure and the shakedown parameter. Calculations were based on typical traction coefficients of 0.43, 0.18 and 0.05 for the unlubricated, water and MIO lubricated cases respectively

steel at a particular depth. Equation (4) is based on the ratchetting threshold for a rolling–sliding Hertzian line contact derived by Kapoor and Williams [**24**] and the orthogonal shear stress, τ_{zx}, which may be calculated using Hertzian contact stress solutions [**25**]. For the current tests, p_s was calculated using the shear yield strength, (k), of the unhardened steel and shear stresses corresponding to traction coefficients typical of those measured during the tests.

Mechanisms S and T both describe growth of an existing defect. Based on the body force method for determining the mode I and II stress intensity factors (SIFs) at the tip of an inclined fluid-filled semicircular crack, Murakami *et al*. [**10**] used an equivalent tensile SIF to describe crack growth by a fluid assisted tensile mechanism. Similarly, Kaneta *et al*. [**11**] used the body force method and an equivalent shear mode SIF to describe shear growth of an inclined semicircular crack, which is controlled primarily by the level of crack face friction; i.e. a lubricant may enter the crack and alter crack face friction, but no fluid pressure is assumed to act. Recently, simple methods have been developed [**26**, **27**] that produce results in good agreement with those from the body force method published by Murakami *et al*. [**10**] and Kaneta *et al*. [**11**] respectively. It was therefore decided to use these simple methods of SIF calculation together with the equivalent SIF methods applied by Murakami *et al*. [**10**] and Kaneta *et al*. [**11**] to predict SIFs for tensile growth of a fluid pressurized crack (mechanism T) and for shear mode crack growth in the absence of fluid pressure (mechanism S). Full details of mechanisms S and T are given elsewhere [**23**, **7**].

Based on the new SIF calculation methods, Fig. 3 shows the variation with crack length (radius) of mechanism S and T stress intensity factors (equivalent shear and tensile mode SIFs respectively [**10**, **11**]) for each of the lubricants (i.e. traction coefficients) used in the experiments. The results shown in Fig. 3 were based on an idealized straight crack at 30° to a contact surface traversed by a fully slipping 1500 MPa Hertzian line contact between two 47 mm diameter test discs. This angle is the shallowest for which the Green's functions, on which the new SIF calculation methods are based, are available. Also shown in Fig. 3 are the threshold stress intensity factors $\Delta K_{\tau\text{th}}$ and $\Delta K_{\sigma th}$ for shear and tensile crack growth, respectively, in carbon steel, which are available from reference [**28**]. The penetration of lubricant into surface-breaking cracks has been demonstrated for similar contact conditions for both water [**9**, **29**] and lubricant MIO [**29**]. The SIFs were calculated for mechanism S during fully lubricated contact (Fig. 3a) and for crack growth following removal of lubricant from the disc surfaces but not from the crack faces (i.e. high surface traction, but crack face friction dependent on the previously applied lubricant, Fig. 3b). The crack face friction coefficients for dry, water and MIO lubricated crack faces were estimated from surface friction coefficients under these conditions, which equal the measured traction coefficients if the contact is assumed to be fully sliding.

To combine mechanisms S, R and T, the TM model (Fig. 4) enables the mechanism appropriate to any rail–wheel contact situation to be identified [**7**]. The mechanism that best describes crack growth for a particular contact condition and crack size is the one for which all the conditions given in the figure are fulfilled, or alternatively it may be predicted that no crack growth will take place. Additional information required to make this decision (stress intensity factors and shakedown limits) is dependent on crack size and contact conditions, and this is discussed further below. Movement from any particular crack growth mechanism to any other is possible to take account of changes in contact or crack tip conditions, so Fig. 4 does not have a linear form. The preference for tensile over shear mode crack growth, when both are possible, derives from the work of Otsuka *et al*. [**28**] and Bogdanski *et al*. [**30**] and is discussed fully in the introduction of the TM model [**7**].

While the TM model aims to identify the most appropriate mechanism to describe crack growth, it does not imply that this mechanism is the only one present. While in the first instance the three mechanisms may, for simplicity, be considered to act independently, it may be necessary that their interaction is considered in cases where, for example, significant strain accumulation due to ratchetting is taking place even when crack growth itself is best described by a shear or tensile mechanism. Although the presence of plasticity may invalidate the application of linear elastic fracture mechanics (LEFM), this can be checked by calculation of the crack tip cyclic plastic zone size, which for plane strain may be estimated using equation (5) [**31**]:

$$2r_{\text{cyclic}} = 0.106\left(\frac{\Delta K}{2\sigma_y}\right)^2 \tag{5}$$

For a crack growing during water lubrication under a 1500 MPa contact pressure (Fig. 3c), equation (5) shows that the cyclic plastic zone size for cracks up to approximately 140 μm long is less than 5 per cent of the crack length, and it is less than 10 per cent of the crack length until the crack exceeds approximately 210 μm in length. Since shakedown ensures that any increment in bulk plastic strain per cycle must be very small, it is not thought to be unreasonable to apply LEFM to a shaken down material. However, it is necessarily only an approximation to the true situation, and the results may not be applicable when crack length exceeds approximately 200 μm for this disc geometry.

3 RESULTS

Numerical data are presented in Table 3. Rail and wheel samples were found to undergo only minimal changes in

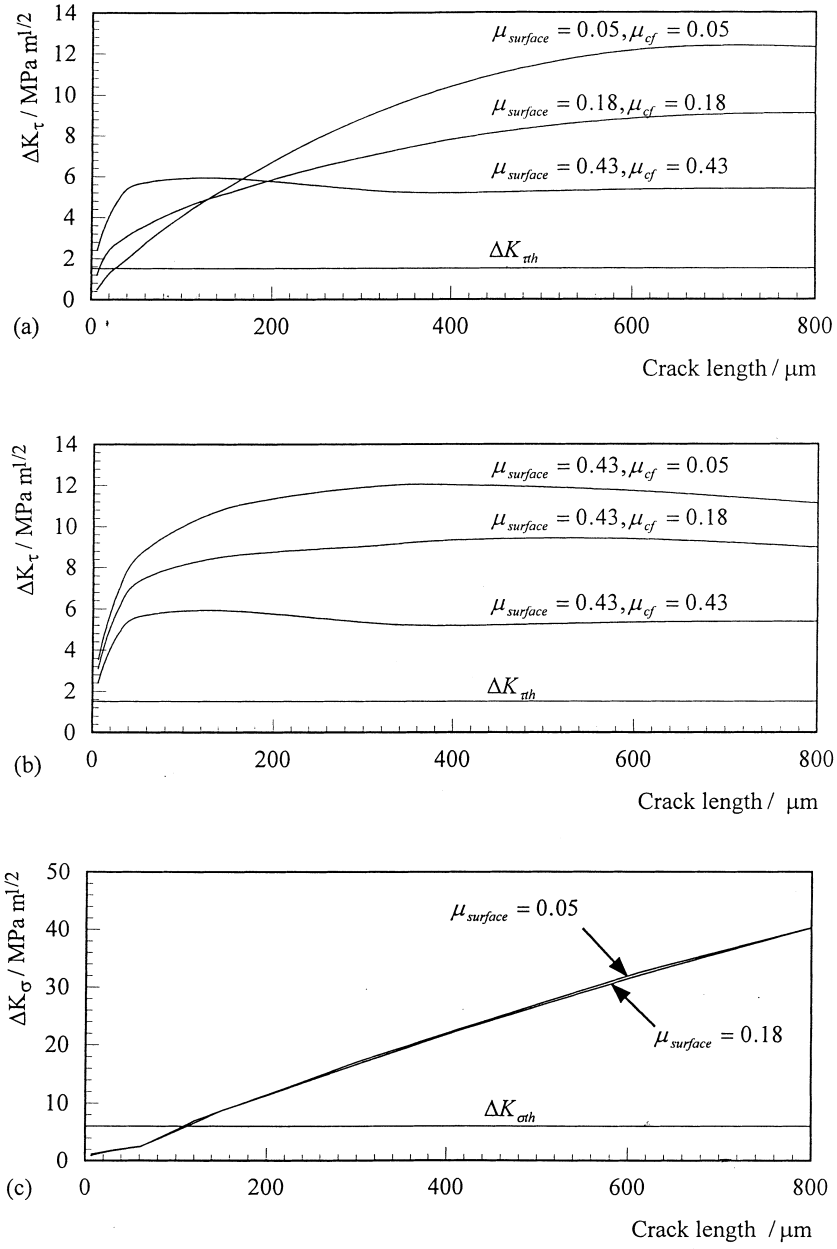

Fig. 3 Variation in stress intensity factor range with crack length (radius) for idealized semicircular cracks at 30° to a contact surface traversed by a fully slipping 1500 MPa Hertzian line contact between two 47 mm diameter test discs. The threshold stress intensities were taken from reference [**22**]. Calculations were based on traction coefficients typical of those measured during the experiments: (a) mechanism S, for a fully lubricated contact with the crack face friction coefficient taken to be equal to the surface traction coefficient; (b) mechanism S, for an unlubricated contact during which crack face friction is influenced by traces of a previously applied lubricant; (c) mechanism T

diameter and mass during testing, and these quantities are not reported since they could not be measured with sufficient accuracy to allow conclusions to be drawn. Crack growth rates were calculated for each test from the length of the largest crack observed at the end of each test divided by the total number of cycles in the test, and therefore represent an average value for the test, including both lubricated and dry periods.

3.1 MIO lubricated contacts

Test M1 ran for 25 000 MIO lubricated cycles, during which the defined disc fatigue life was not reached, and was then stopped. The subsurface strain in the rail steel following these cycles can be seen in Fig. 5a. The pattern of strain accumulation was consistent with the depths at which Fig. 2 shows the applied contact pressure to be

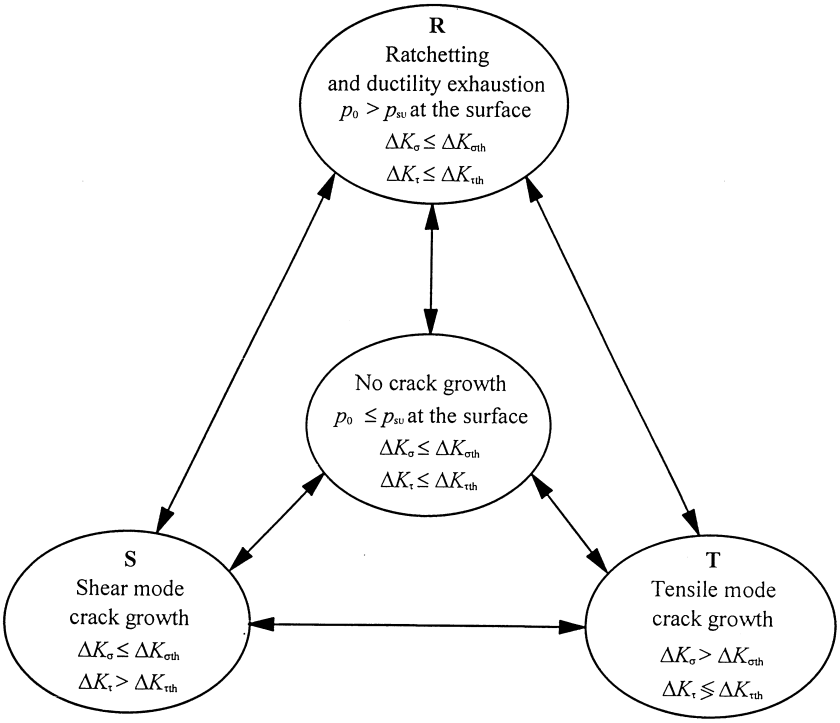

Fig. 4 Three-mechanism (TM) model of rolling contact fatigue crack growth. The criteria in the diagram may be used to predict the mechanism by which rolling contact fatigue crack growth will take place, or alternatively, it may be predicted that no crack growth will take place for a particular loading condition

above the shakedown parameter of the steel, p_S^M. Although no large fatigue cracks formed during the test, damage of the type shown in Fig. 5b was typical of that found at the surface of the disc. Damage was generally, but not exclusively, associated with near-surface inclusions in the steel, and had typical dimensions of 4 μm in length and 1.5 μm in depth.

The rail disc in test M2 reached the defined fatigue life after approximately 44 000 cycles. The maximum crack length observed in the rail sample was 1030 μm,

Table 3 Test results

Test code	Test duration incuding dry phase (rail cycles)	Maximum crack length observed in rail disc (μm)	Maximum crack depth observed in rail disc (μm)	Appropriate growth angle at crack mouth (deg)	Growth rate nm/cycle)
M1	25 000*	7	3	20	0.3
M2	43 966†	1030	360	20	23
M3	28 895†	1500	300	10	52
M4	25 497†	1430	110	5	56
M5	25 500†	260	7	5	10
M6	25 246*	110	8	5	4
W1–W4‡	10 138†	1260	515	20	112
W5	11 782†	815	360	25	69
W6	9608†	720	340	30	75
W7	6001*	43	7	8	7
W8	6252*	45	6	10	7
D1	249*	73	6	2	293
D2	499*	61	11	10	122

* Test stopped at a predetermined number of cycles.
† Test stopped at the defined fatigue life.
‡ Results are the average of tests W1 to W4 which took place under identical conditions.

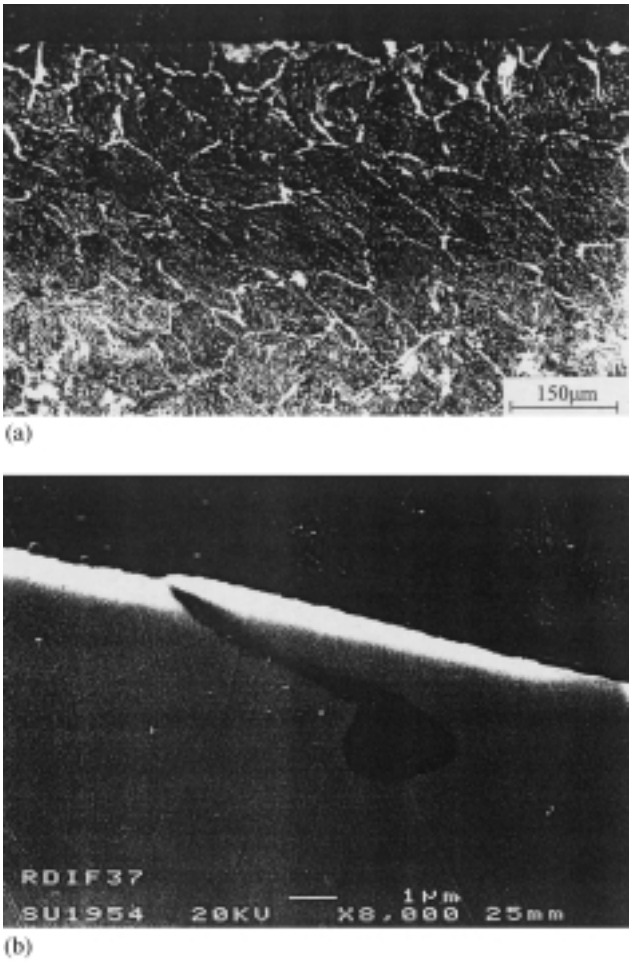

Fig. 5 (a) Optical micrograph of a section of the rail disc from test M1, showing that ratchetting has taken place below the disc surface, leading to distortion of the microstructure of the steel. (b) SEM micrograph of a section of the rail disc from test M1. A small crack exists at a shallow angle beneath the disc surface and is linked to an inclusion lying below the surface of the disc

although further smaller cracks were found that had a similar morphology to this large crack. Test D2 (500 unlubricated cycles) showed that, after the initial unlubricated period, cracks of around 60 μm long would have been present, so the majority of the crack growth in test M2 took place during the lubricated period. The average crack growth rate for test M2 is therefore a reasonable estimate of the growth rate under lubricated conditions following unlubricated cycles. Comparison of crack growth rates during tests M1 and M2 (Table 3) shows that the addition of a period of unlubricated contact at the start of the test significantly accelerated the crack growth rate during the lubricated cycles, as would be expected from previous experience in water lubricated conditions [**8**].

Following test M2, subsurface plastic deformation due to the low-traction lubricated cycles was present, in addition to surface deformation produced during the initial high-traction dry cycles. The deformation observed was consistent with the depths at which the applied contact pressure exceeded the shakedown parameters p_s^D and p_s^M.

In test M3, rail surface failure took place during the second period of dry cycles by the formation of tears in the surface of the disc (Fig. 6a) which just failed to produce fatigue life signals on the eddy current crack detection equipment. Prior to this, at the end of the first lubricated period, there had been no significant cracks indicated by the eddy current system. Following reapplication of the lubricant, it was found that eddy current signals developed very quickly, and the fatigue life was reached within 3650 additional cycles. Examination of the disc at this point revealed the unbranched and blunt crack shown in Fig. 6b.

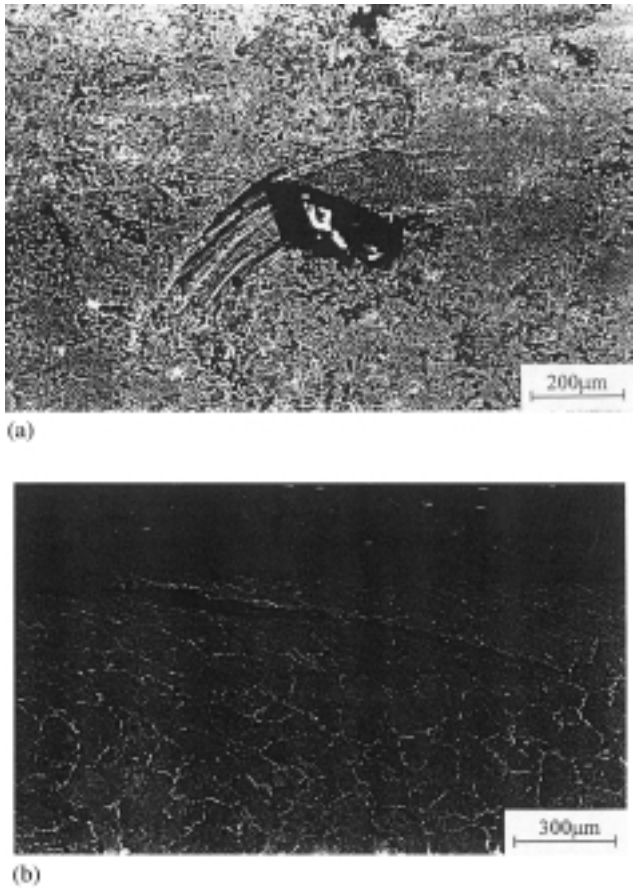

Fig. 6 Optical micrographs of (a) the surface of the rail disc from test M3, showing a surface tear produced during the second period of unlubricated contact, and (b) a section from the rail disc from test M3, showing a crack observed after the second lubricated period of the test

Because the rail disc surface failure observed in test M3 was unusual, the test was repeated (test M4), and this revealed exactly the same behaviour as found during test M3. A further repeat of the test (M5) using an ultrasonic lubricant removal technique made little difference to the result, and the rail disc in test M5 suffered surface tearing almost identical to that seen during tests M3 and M4, although the observed crack was shorter in this case. The subsurface strains observed following tests M3 to M5 were consistent with the depths at which the applied maximum Hertzian contact pressure exceeded the shakedown parameters p_s^D and p_s^M.

The effect of reversing the sequence of the lubricated and dry periods used in tests such as M3 was examined in test M6. During the lubricated period of contact, no crack development was indicated by the eddy current system, as would be expected from the result of test M1. When the lubricant was removed, the following unlubricated cycles led to visible disc surface damage which was similar to that formed during the second dry period of tests M3 to M5, although it was not as severe. An optical micrograph of the region below one of the tears formed on the disc surface showed a defect around 110 μm long and 8 μm deep. Viewing the section taken from the disc using the SEM revealed several similar defects with a typical size of 55 μm long and 8 μm deep. Deformation of the rail steel was again consistent with the shakedown curves p_s^M and p_s^D (Fig. 2) for the low- and high-traction cycles, respectively, used during the test.

Traction coefficient development was almost identical during each of tests M3 to M5, as would be expected since they were carried out under identical conditions, and is shown for test M3 in Fig. 7a. It can be seen that the second dry period began with a coefficient of traction higher than that at the start of the first dry period of the test, and this rose to around 0.43 during the second period of 250 dry cycles. The traction coefficient during application of MIO was around 0.05 for each of tests M1 to M6.

3.2 Water lubricated contacts

Tests W1 to W4 were carried out under identical conditions, with all 500 unlubricated cycles at the start of the test. The average fatigue life for these tests was 10 138 cycles, with deviations of +1120 and −1178 cycles, indicating the high reproducibility of the SUROS test machine. Tests W1 to W4 showed that an initial 500-cycle unlubricated period followed by water lubrication produced large cracks (nearly 3 times the contact half-width long, and over 1.5 times the contact half-width deep) which included some minor branches but maintained a dominant growth path at around 20° to the rail steel surface (Fig. 8).

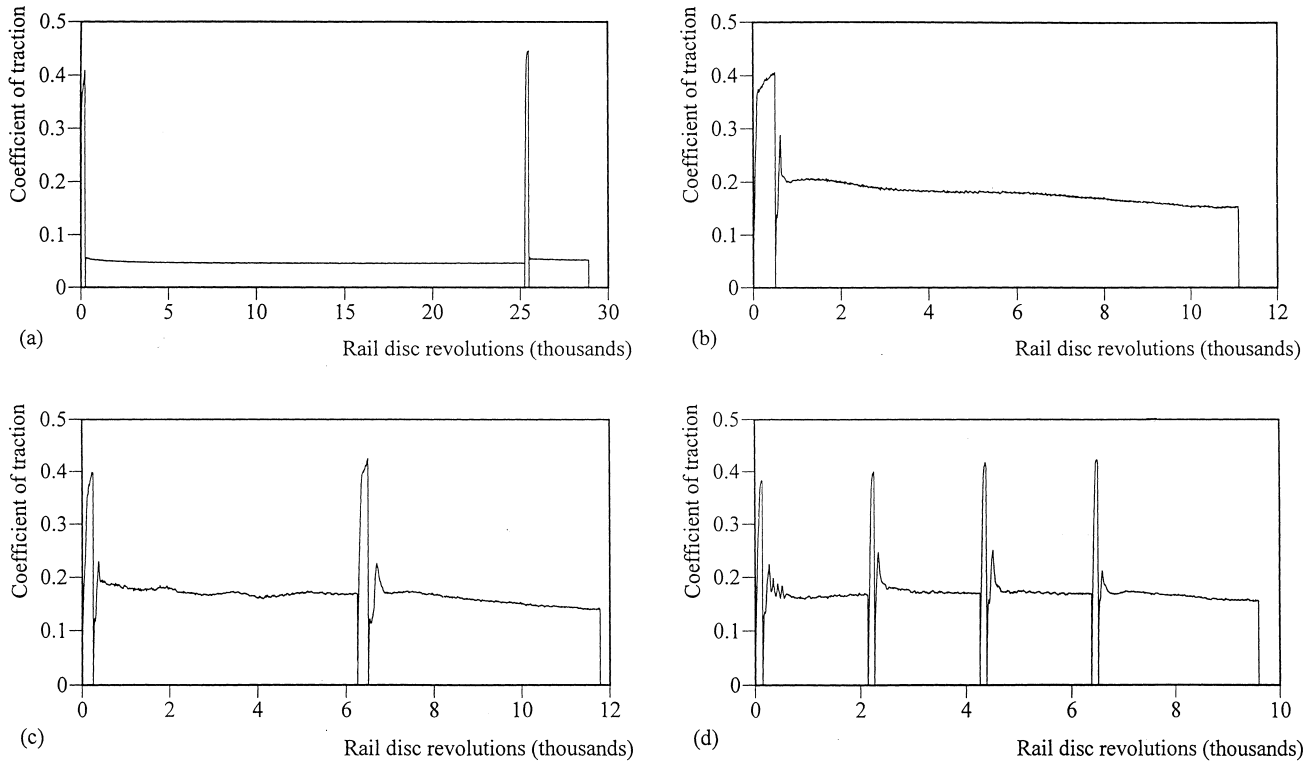

Fig. 7 Traction coefficient plotted against the number of rail disc revolutions for tests (a) M3, (b) W4, (c) W5 and (d) W6

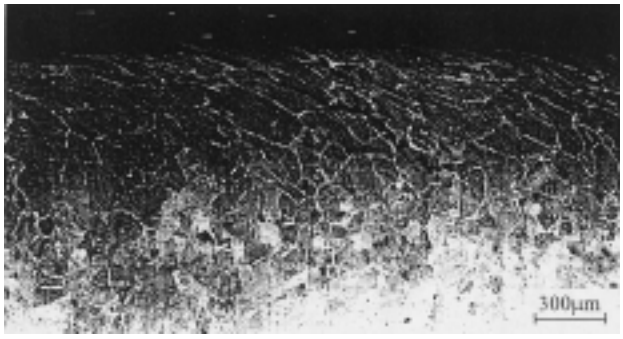

Fig. 8 Optical micrograph of a section of the rail disc from test W3. The combination of unlubricated and water lubricated cycles has produced both surface and subsurface deformation of the steel

Test W5 showed that splitting the 500 unlubricated cycles into two groups of 250 cycles separated by 6000 water lubricated cycles made no significant difference to the fatigue life of the disc. However, a section taken from rail test disc W5 revealed a crack that was shorter and shallower than those found following tests W1 to W4, but that had developed at a similar angle and with similar morphology. Test W6 (four groups of 125 cycles separated by 2000 water lubricated cycles) gave a slightly lower fatigue life, but the reduction was not thought to be significant since the fatigue life remained within the range found during tests W1 to W4. The morphology of the crack was similar to that of the cracks grown during tests W1 to W4, and its size was comparable to that found following test W5.

Figures 7c and d show that in each consecutive unlubricated period of tests W5 and W6 the traction coefficient reached a slightly higher level, and by the end of the last dry period of each test it had reached a value similar to that at the end of the continuous 500-cycle unlubricated period at the start of test W4 (Fig. 7b, typical of behaviour during tests W1 to W4). With the exception of the transient effects of restarting after each unlubricated period, the traction coefficient during the water lubricated stages of the intermittent lubrication tests was virtually unaffected by the intervening dry cycles. The deformation of the steel appeared similar in all of tests W1 to W6. It was consistent with the combination of high-traction unlubricated cycles and lower-traction water lubricated cycles, and correlated well with the shakedown curves p_s^D and p_s^W for these conditions (Fig. 2).

Tests W7 and W8 both ran for 6000 water lubricated cycles, and in test W8 these were followed by an additional 250 dry cycles. No cracks were detected by the eddy current system in either test, but small cracks (Table 3) were revealed when the sectioned specimens were examined using the SEM. Optical micrographs of etched sections revealed deformation consistent with the traction levels that had been applied during the tests and the corresponding shakedown parameters. The surface deformation induced by the additional 250 dry cycles in test W8 is clear from the micrographs in Fig. 9.

4 DISCUSSION

For a surface and crack face friction coefficient of 0.05 (characteristic of MIO lubrication) it can be predicted using the TM model (Figs 3 and 4) that crack growth

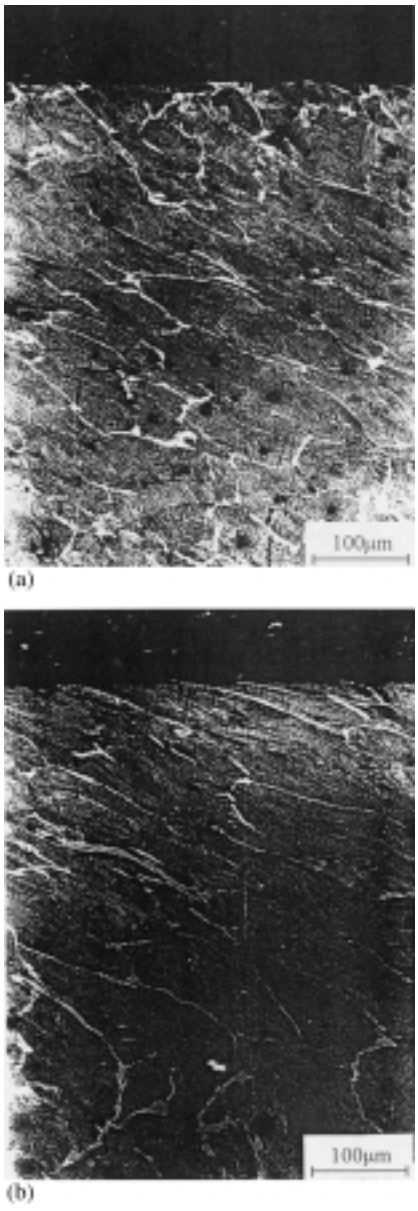

Fig. 9 Optical micrographs of sections of the rail discs from tests (a) W7 and (b) W8. Tests W7 and W8 were identical except for an additional 250 unlubricated cycles applied at the end of test W8. The additional near-surface deformation produced by these cycles can be seen by comparison of (a) and (b)

will be by mechanism S ($\Delta K_\tau > \Delta K_{\tau th}$ but $\Delta K_\sigma \leqslant \Delta K_{\sigma th}$) for crack lengths of approximately 26–110 μm, and by mechanism T ($\Delta K_\sigma > \Delta K_{\sigma th}$) for crack lengths above 110 μm. For a surface and crack face friction coefficient of 0.18 (characteristic of water lubrication) the corresponding lengths are 9–110 μm for mechanism S and, again, over 110 μm for mechanism T.

During tests M1 and W7, in which lubricants were applied throughout testing, cracks developed in the higher-traction water lubricated test that were over 6 times the length of those found in the lower-traction MIO lubricated test, even though the duration of the latter was over 4 times that of test W7. The traction coefficient during MIO lubrication was sufficiently low for ratchetting at the surface of the disc to be prevented (i.e. $p_0 < p_s^M$, Fig. 2), thereby preventing the development of surface defects in the disc (with the exception of the small defects associated with subsurface inclusions, or possibly high local stresses due to asperity contacts). In the case of the water lubricated disc, test W7, ratchetting at the surface of the disc was possible (i.e. $p_0 > p_s^W$), so initial crack development could take place.

For tests M1 and W7 the TM model predicts that the MIO lubricant prevented the development of defects large enough for mechanism S crack growth to begin, whereas water allowed such defects to develop, leading to the possibility of larger-scale crack growth. The result of test M1 is consistent with previous tests carried out under similar conditions by Clayton and Hill [**32**], which showed that, after 1.5 million cycles, no fatigue damage could be found in rolling contact specimens that were continuously lubricated by graphite or MoS_2.

The dependence of crack growth on ratchetting during lubricated contact was removed in tests M2 and W1 to W4, in which a 500-cycle unlubricated period produced initial defects, the size of which may be estimated from test D2, prior to the application of MIO and water lubricants respectively. Applying the TM model to test sequences M2 and W1 to W4 shows that for both lubricant types the size of these initial defects exceeded the minimum size required for mechanism S crack propagation, so the extensive crack growth observed could have been predicted.

The difference in rail steel fatigue life found between tests M2 and W1 to W4 may be linked to the crack growth mechanisms identified by the TM model. Figure 3c shows that ΔK_σ is virtually independent of the surface traction coefficient for the crack lengths considered, and it may therefore be assumed that the rate of crack growth driven by mechanism T will be independent of surface traction (i.e. lubrication type) for a particular crack length. If it is assumed that the initial unlubricated cycles eliminated the requirement for further ratchetting prior to mechanism S crack growth, the difference in the fatigue lives found between tests M2 and W1 to W4 (which were identical except for the lubricant used) may be explained by a difference in the rate of crack propagation during the mechanism S stage of crack growth, when the cracks were between approximately 60 and 110 μm long. Figure 3a confirms that this is a possibility, since, for the relevant crack lengths, ΔK_τ is higher for water lubrication than for MIO lubrication. However, since no measurements of crack length were attempted during tests M2 or W1 to W4 (the eddy current equipment is not capable of such quantified measurements), it is not possible to verify the explanation suggested above.

Having identified that the predictions of the TM model appear plausible for the lubricant application sequences used during tests M1 and M2, W1 to W4 and W7, the following discussion considers the more complex tests involving intermittent lubrication. During unlubricated periods following lubricant removal it was thought that lubricant may have remained inside surface-breaking cracks, even after ultrasonic disc cleaning, and this was confirmed by energy dispersive X-ray spectroscopy (EDS) analysis of cracks from MIO lubricated tests [**29**]. However, although traces of lubricant were detected inside the cracks, the quantities involved were known to have been low since no seepage of lubricant from the cracks was detected and the traction was high during the unlubricated periods. (The coefficient of traction is sensitive enough to be changed significantly even by the grease from a finger print, and would have indicated the presence of any lubricant on the disc surface.) While these traces of lubricant were thought insufficient to support crack propagation by mechanism T, they may have been sufficient to alter crack face friction levels. The importance of this possibility is illustrated by Fig. 3b for mechanism S, which shows that with high surface traction the stress intensity factor range, ΔK_τ, increases dramatically as the level of crack face friction is reduced for any given crack length.

An initial unlubricated period of 250 cycles was shown by test D1 to produce defects of approximately 70 μm long, for which Fig. 3a shows that the threshold SIF value calculated by Otsuka *et al.* [**28**] will be exceeded on application of a lubricant. As for tests M2 and W1 to W4, the application of dry cycles at the start of tests M3 to M5 and W5 may therefore be assumed to have eliminated the requirement for further ratchetting before mechanism S crack growth could begin. During the first lubricated period of tests M3 to M5 and W5, crack growth is therefore predicted by the TM model, with ΔK_τ for water lubrication exceeding that for MIO lubrication (Fig. 3a) while the cracks remain below 110 μm long, the length at which mechanism T propagation is predicted to begin. However, following removal of the lubricant from the contact surfaces, although ΔK_τ rises for both lubricant types, the situation is reversed. Figure 3b shows that, during high-traction contact, a crack containing traces of lubricant MIO, and exceeding approximately 80 μm in length, will have a larger value of ΔK_τ present at its tip than will a crack containing a trace of water, whatever the length of

the water lubricated crack, within the range considered. Although the levels of crack face friction can only be estimated, and the angle of crack growth varied between the tests, this shows that mechanism S, with crack face friction variation due to traces of previously applied lubricants, is a mechanism that may explain why rapid crack growth (i.e. relatively high ΔK_τ) and surface tearing occurred during the intermittently lubricated MIO tests M3 to M5 but not during the intermittently water lubricated tests W5 and W6.

Results from the additional tests W7 and W8 further support the results of tests W1 to W6 by showing that the application of 250 unlubricated cycles following water lubrication produced no significant crack growth, or any growth was minimal and was masked by variation in the initial defect size estimated from test W7. However, during test M6, only very small defects (approximately 7 μm long and 3 μm deep, estimated from the results of test M1) were present before the application of 250 dry cycles, yet the cracks present immediately after the unlubricated period were both deeper and longer than those found after a similar number of dry cycles at the start of a test, estimated from test D1. As for the tests described above, it is thought that variation in ΔK_τ owing to modification of crack face friction by lubricant remaining in small surface-breaking cracks may help to explain these results.

If interruption of lubrication for full-scale rail–wheel contacts were found to produce results similar to those from the laboratory-based tests described above, it is possible that the perhaps unavoidably imperfect application of liquid-based flange lubricants could promote crack growth in rails. A solution to this potential problem may be offered by solid lubricants. Laboratory tests have shown that solid wheel flange lubricants have reduced rail steel wear to significantly lower levels than would be expected for an unlubricated contact, but were found to lead to rail steel failure by wear rather than RCF [**33**]. It is thought that solid lubricants are less likely than liquid lubricants to enter surface-breaking cracks, and are therefore less likely to accelerate crack growth through reduction of crack face friction.

5 CONCLUSIONS

Tests were carried out to investigate the effects on rail rolling contact fatigue of intermittent lubrication which may occur owing to unreliable flange lubricators. Intermittent lubrication of a simulated rail–wheel contact revealed an important and rapid mode of rail steel surface failure following MIO lubrication that was not found during similar experiments using water. The three-mechanism model of rail rolling contact fatigue, comprising ratchetting, shear mode and tensile mode crack growth mechanisms, was used to examine the results, which were found to be in general agreement with the model.

ACKNOWLEDGEMENTS

The supply of materials by ADtranz Wheelset Division, British Steel Track Products and Acheson Colloids Limited is greatly appreciated. Financial support for the project was provided by the University of Sheffield and the Advanced Railway Research Centre (ARRC).

REFERENCES

1 **Allery, B. P.** Improvements in rail maintenance techniques and manufacturing processes. *Proc. Instn Civ. Engrs Transp.*, 1993, **100**, 227–230.
2 **Thelen, G.** and **Lovette, M.** A parametric study of the lubrication transport mechanism at the wheel/rail interface. *Wear*, 1996, **191**, 113–120.
3 **Cantera, F.** Investigation of wheel flange wear in Santander FEVE rail–a case study. *Wear*, 1993, **162**, 975–979.
4 **Way, S.** Pitting due to rolling contact. *Proc. ASME, J. Appl. Mechanics*, 1935, **2**, A49–A55.
5 **Keer, L. M.** and **Bryant, M. D.** A pitting model for rolling contact fatigue. *Proc. ASME, J. Lubric. Technol.*, 1983, **105**, 198–205.
6 **Bower, A. F.** The influence of crack face friction and trapped fluid on rolling contact fatigue cracks. *Proc. ASME, J. Tribology*, 1988, **110**, 704–711.
7 **Fletcher, D. I.** and **Beynon, J. H.** The effect of contact load reduction on the fatigue life of pearlitic rail steel in lubricated rolling–sliding contact (to appear in *Fatigue Fract. Engng Mater. Struct.*, 2000).
8 **Tyfour, W. R., Beynon, J. H.** and **Kapoor, A.** Deterioration of the rolling contact fatigue life of pearlitic rail steel due to dry–wet rolling–sliding line contact. *Wear*, 1996, **197**, 255–265.
9 **Kaneta, M., Matsuda, K., Murakami, K.** and **Nishikawa, H.** A possible mechanism for rail dark spot defects. *Proc. ASME, J. Tribology*, 1998, **120**, 304–309.
10 **Murakami, Y., Kaneta, M.** and **Yatsuzuka, H.** Analysis of surface crack propagation in lubricated rolling contact. *ASLE Trans.*, 1985, **28**, 60–68.
11 **Kaneta, M., Yatsuzuka, H.** and **Murakami, Y.** Mechanism of crack growth in lubricated rolling/sliding contact. *ASLE Trans.*, 1985, **28**, 407–414.
12 **Fletcher, D. I.** and **Beynon, J. H.** Development of a machine for closely controlled rolling contact fatigue and wear testing under high stress conditions. *ASTM J. Test. Eval.*, 2000, **28**(4), 267–275.
13 **Beynon, J. H., Garnham, J. E.** and **Sawley, K. J.** Rolling contact fatigue of three pearlitic rail steels. *Wear*, 1996, **192**, 94–111.
14 **Clayton, P.** and **Su, X.** Surface initiated fatigue of pearlitic and bainitic steels under water lubricated rolling/sliding contacts. *Wear*, 1996, **200**, 63–73.
15 **Garnham, J. E.** and **Beynon, J. H.** The early detection of rolling–sliding contact fatigue cracks. *Wear*, 1991, **144**, 103–116.

16 **Timoshenko, S. P.** and **Goodier, J. N.** *Theory of Elasticity*, 3rd edition, 1970, pp. 403-420 (McGraw-Hill, London).
17 **Kalousek, J.** Wear and contact fatigue model for railway rail. Technical Report 1986/10, National Research Council of Canada, Canada, 1986.
18 **Barwell, F. T.** The tribology of wheel on rail. *Tribology Int*., 1974, **7**, 146–150.
19 **Bolton, P. J.** and **Clayton, P.** Rolling-sliding wear damage in rail and tyre steels. *Wear*, 1984, **93**, 145–165.
20 **Greenwood, J.** The contact of real surfaces. In Proceedings of International Symposium on *Contact Mechanics and Wear of Wheel/Rail Systems*, University of British Columbia, Vancouver, Canada, 1982, pp. 21–37.
21 **Kapoor, A.** and **Johnson, K. L.** Plastic ratchetting as a mechanism of metallic wear. *Proc. R. Soc. (Lond.) A*, 1994, **445**, 367–381.
22 **Kapoor, A.** A re-evaluation of the life to rupture of ductile metals by cyclic plastic strain. *Fatigue Fract. Engng Mater. Struct*., 1994, **17**, 201–219.
23 **Fletcher, D. I.** and **Beynon, J. H.** Equilibrium of crack growth and wear rates during unlubricated rolling–sliding contact of pearlitic rail steel. *Proc. Instn Mech. Engrs, Part F, Journal of Rail and Rapid Transit*, 2000, **214**(F2), 93–105.
24 **Kapoor, A.** and **Williams, J. A.** Shakedown limits in sliding contacts on a surface-hardened half-space. *Wear*, 1994, **172**, 197–206.
25 Engineering Sciences Data Unit, Item 85007 Contact Phenomena III, ESDU International, London, 1994.
26 **Fletcher, D. I.** and **Beynon, J. H.** A simple method of stress intensity factor calculation for inclined fluid-filled surface-breaking cracks under contact loading. *Proc. Instn Mech. Engrs, Part J, Journal of Engineering Tribology*, 1999, **213**(J4), 299–304.
27 **Fletcher, D. I.** and **Beynon, J. H.** A simple method of stress intensity factor calculation for inclined surface breaking cracks with crack face friction under contact loading. *Proc. Instn Mech. Engrs, Part J, Journal of Engineering Tribology*, 1999, **213**(J6), 481–486.
28 **Otsuka, A., Mori, K.** and **Miyata, T.** The condition of fatigue crack growth in mixed mode condition. *Engng Fract. Mechanics*, 1975, **7**, 429–439.
29 **Fletcher, D. I.** The influence of lubrication on the fatigue of pearlitic rail steel. PhD thesis, University of Sheffield, 1999.
30 **Bogdanski, S., Stupnicki, J., Brown, M. W.** and **Cannon, D. F.** A two dimensional analysis of mixed-mode rolling contact fatigue crack growth in rails. In Proceedings of 5th International Conference on *Biaxial/Multiaxial Fatigue and Fracture*, Krakow, 1997, pp. 189–206.
31 **Dowling, N. E.** *Mechanical Behaviour of Materials*, 1993 (Prentice-Hall International, New Jersey).
32 **Clayton, P.** and **Hill, D. N.** Rolling contact fatigue of a rail steel. *Wear*, 1987, **117**, 319–334.
33 **Fletcher, D. I.** and **Beynon, J. H.** The influence of lubricant type on rolling contact fatigue of pearlitic rail steel. In Proceedings of 25th Leeds–Lyon Symposium on *Tribology*, Lyon, 8–11 September 1998, 1999, pp. 299–310 (Elsevier Science).